

Nuclear tetrahedral states and high-spin states studied using quantum number projection method

S Tagami, M Shimada, Y Fujioka, Y R Shimizu

*Department of Physics, Faculty of Sciences,
Kyushu University Fukuoka 812-8581, Japan*
and

J Dudek

*Institut Pluridisciplinaire Hubert Curien (IPHC),
IN2P3-CNRS/Université de Strasbourg, F-67037 Strasbourg, France*

PACS REF: 21.10.Re, 21.60.Ev, 21.60.Jz, 23.20.Lv

Abstract

We have recently developed an efficient method of performing the full quantum number projection from the most general mean-field (HFB type) wave functions including the angular momentum, parity as well as the proton and neutron particle numbers. With this method, we have been investigating several nuclear structure mechanisms. In this report, we discuss the obtained quantum rotational spectra of the tetrahedral nuclear states formulating certain experimentally verifiable criteria, of the high-spin states, focussing on the wobbling- and chiral-bands, and of the drip-line nuclei as illustrative examples.

1. Introduction

In the studies of the nuclear structure problems, especially of the nuclear collective motion, the underlying observables are the energy spectra and the transition rates. Although the mean-field methods, such as the Hartree-Fock (HF) or the Hartree-Fock-Bogoliubov (HFB) method, or more recently, the energy density functional (EDF) theories have been making remarkable progress, nevertheless some further steps are necessary to obtain the experiment-comparable information. These involve in particular, the quantum number projection techniques, which require even nowadays considerable numerical efforts.

We have developed recently an efficient method to perform quantum number projections [1]. In this contribution, we would like to show and discuss some results of our recent studies which employ the projection method. Ultimately, the framework of our approach is the standard one, according to which the total wave function is described by the linear combination of the projected states,

$$|\Psi_{M;\alpha}^{INZ(\pm)}\rangle = \sum_{K,n} g_{K,n,\alpha}^{INZ(\pm)} \hat{P}_{MK}^I \hat{P}_{\pm}^N \hat{P}^Z |\Phi_n\rangle, \quad (1)$$

where $|\Phi_n\rangle$ are the symmetry-broken HFB-type wave functions, and \hat{P}_{MK}^I , \hat{P}_{\pm}^N , and \hat{P}^Z are the angular momentum, the parity, and the neutron and proton number projectors, respectively. The coefficients of the linear combination, $g_{K,n,\alpha}^{INZ(\pm)}$, are obtained by solving the so-called

Hill-Wheeler equation, see e.g. [2] for the detailed formulation. In the present work we only discuss the results with one HFB state, i.e., without the configuration mixing of the generator coordinate method (GCM).

2. Efficient method for projection

The basic features of our method [1] for projection (and GCM) are summarised as follows: 1) The most general symmetry-broken HFB-type state can be treated including the breaking of time-reversal symmetry (cranking), and the method can be applied not only to the even-even but also to odd and odd-odd nuclei. 2) The harmonic oscillator basis is used at present, but a new basis of the Gaussian expansion, which is more suitable for the weakly bound system (halo/skin), is under development. 3) The truncation scheme based on the canonical basis is efficiently employed. 4) The Thouless amplitude $Z_{ll'}$ with respect to the Slater determinant state is used,

$$|\Phi\rangle = \exp\left(\sum_{ll'} Z_{ll'} a_l^\dagger a_{l'}^\dagger\right) |\phi_0\rangle, \quad |\phi_0\rangle = \prod_{k=1}^N b_k^\dagger |0\rangle, \quad (2)$$

where N is the number of particles, and $a_k^\dagger = b_k$ ($k \leq N$) or $a_k^\dagger = b_k^\dagger$ ($k > N$) with b_k^\dagger being the canonical basis creation operator of HFB-type state $|\Phi\rangle$. In this way, we can treat the situation of weak-pairing case without any problem ($Z \rightarrow 0$), and can easily adopt the Pfaffian formula [3] for calculating overlaps.

As for the Hamiltonian, we employ the Woods-Saxon single-particle potential and the schematic separable-type residual interactions. For the particle-hole channel, we take the multipole interaction ($\lambda = 2, 3, 4$), whose form factor is the derivative of the Woods-Saxon potential, with the selfconsistent value of the strength as in §6-5 of Ref. [4] (no fitting at all). For the pairing channel, we take the usual multipole-type (the r^λ form factor) with $\lambda = 0$ and 2, where the monopole (quadrupole) pairing strength is fixed to reproduce the even-odd mass-differences (moment

of inertia of the ground state band), see Ref. [1] for details. Quite recently we have been able to perform the projection calculation making use of the more realistic Gogny force (the D1S parametrisation). We will show a few preliminary results with it, while in most of the calculations we will employ the Woods-Saxon potential with the schematic multipole interaction schematised above (“WS+MI”).

Here we would like to emphasise the importance of the cranking term, in our case, $-\omega_{\text{rot}}J_x$, to generate the mean-field state sufficiently rich in terms of various-symmetry states as a ‘trial function to project from’, especially for the ground state band. In the axially symmetric ground state, the mean-field wave function contains only $K = 0$ component without cranking. The cranking term induces the $K = \pm 1$ (time-odd) components, which increase the moment of inertia considerably (by 30–40%): For this purpose, small cranking frequency is enough, e.g., $\hbar\omega_{\text{rot}}$ of the order of a few 10’s of keV, and the results do not depend on a chosen value of the frequency as long as it is sufficiently small; see Fig. 7 and 8 of Ref. [1].

3. Tetrahedral nuclear states

Our first application of the projection method will be to study the tetrahedral-symmetry in certain nuclear states. In the nuclear structure context the tetrahedral symmetry, T_d , is sometimes referred to as *high-rank* point-group symmetry to stress the existence of the 4-dimensional irreducible representation of this group implying the four-fold degeneracy of certain nucleonic levels. The latter mechanism leads to the extra nuclear stability due to the specific shell effect (see below).

Tetrahedral shapes can be most easily described as α_{32} -deformation in the usual nuclear surface parameterisation $R(\theta, \varphi) \propto [1 + \sum \alpha_{\lambda\mu}^* Y_{\lambda\mu}(\theta, \varphi)]$. When the single-particle orbitals, $\{\psi_n, e_n\}$, are calculated in function of the tetrahedral deformation α_{32} , the existence of four-fold degenerate energy levels in addition to the usual two-fold degenerate ones contributes to the appearance of large shell gaps at certain nucleon numbers, i.e., there exist “tetrahedral closed shells”, see e.g. [5]. The presence of the multipolarity $\lambda = 3$ implies that the parity is broken in the nuclear intrinsic frame of reference and the presence of Y_{32} in $R(\theta, \phi)$ above implies that the axial-symmetry is broken. Thus, with the cranking term, the single-particle Hamiltonian has almost none of the otherwise often present mean-field symmetries, and the general projection procedure of Eq. (1) is indeed necessary.

The question arises: What are the specific properties of spectra generated by tetrahedral-symmetric Hamiltonian? We have recently performed the projection calculations for the tetrahedral closed shell nuclei [6]. The tetrahedral shape is realised in molecular physics, e.g., in the methane (CH_4), the latter known as a tetrahedral rotor. Paradoxically, it is a kind of “spherical rotor” in the sense that all the three principal-axis moments of inertia are the same. However, the group theory tells us that only some specific

spin-parity combinations are allowed in the quantum spectra of the tetrahedral rotors according to irreducible representations of the T_d symmetry group. The ground state rotational sequence of the tetrahedral double-closed shell nuclei belongs to the so-called A_1 representation, whose spin-parity combinations form the following sequence

$$A_1 : \begin{array}{l} 0^+, 3^-, 4^+, 6^+, 6^-, 7^-, 8^+, 9^+, 9^-, \\ 10^+, 10^-, 11^-, 2 \times 12^+, 12^-, \dots \end{array} \quad (3)$$

Indeed we have shown that the results of the projections precisely follow this property, see Fig. 2 of [6]. Furthermore, for small tetrahedral deformations the spectra are approximately equidistant, resembling the multi-phonon structure based on the 3^- phonon. This energy-spin dependence gradually changes to the $E_I \sim I(I+1)$ type dependence, when tetrahedral deformation increases, i.e., the transition from vibrational-like to rotational spectra is clearly seen [6].

Among tetrahedral double-closed shell nuclei, ^{80}Zr is one of the most prominent. Our recent Gogny D1S HFB calculations suggest that the ground state has the tetrahedral deformation $\alpha_{32} = 0.11 - 0.12$, which has lower energy than the prolate deformed minimum with $\beta \approx 0.45$ by more than 3 MeV. Our phenomenological mean-field calculations with the deformed Woods-Saxon potential, cf. figure 1, predict that within limited deformation space of quadrupole and hexadecapole deformations, the ground-state is expected to be very strongly deformed (‘superdeformed’) with $\beta \approx 0.43$. However, when the minimisation over the tetrahedral deformation is allowed, the energy landscape changes dramatically, the spherical minimum disappears and the tetrahedral-symmetry minima appear for $\alpha_{32} \approx \pm 0.2$, about 3.2 MeV below.

The doubly-magic tetrahedral nucleus $^{80}_{40}\text{Zr}_{40}$ is a very exotic one. Whereas experimentally only one rotational band is known, with clearly identified $E2$ -transitions, no experimental data exist for the lighter isotopes. Given the fact that *strictly tetrahedral-symmetric* configurations generate neither quadrupole nor dipole moments, the population and observation of tetrahedral rotational bands belongs to the realm of ‘rare events’, therefore most likely not yet seen. For this reason the theory predictions from various independent calculations and models indicating coherently that the ground-states in ^{80}Zr has tetrahedral symmetry deserves attention when planning new experiments. As we believe, it is very likely that the observed ‘superdeformed’ band is an excited one, whereas the tetrahedral symmetric ground-state band has never been seen. Since the tetrahedral configurations generate in turn strong octupole moments, the future experiments should possibly aim at this observable, if not in the very exotic ^{80}Zr , whose population may cause extra problems with the statistics, then perhaps in some other isotopes in which similar properties are predicted.

The pairing correlations are quenched for both neutrons and protons because of the large shell gaps at $N = Z = 40$. In figure 2 we show our preliminary result of spectrum with

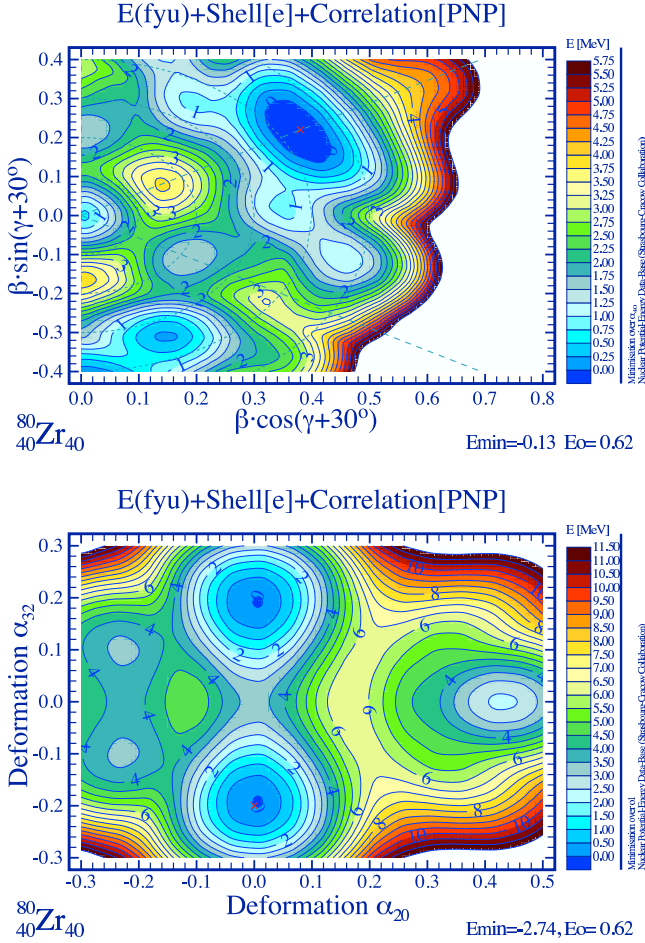


Fig. 1: According to the phenomenological mean-field calculations with the Woods-Saxon Hamiltonian (universal parameterisation) the ‘superdeformed’ minimum, top, is the lowest in energy; here at each $\{\beta, \gamma\}$ point the minimisation was performed over α_{40} . When the extra minimisation over tetrahedral (α_{32}) deformation is allowed, bottom, the spherical minimum disappears, and the nucleus arrives at the tetrahedral deformation minima with $\alpha_{32} \approx \pm 0.2$, gaining 3.2 MeV, in an excellent agreement with our Gogny calculations. [From [7]].

the Gogny D1S force as an example, where the oscillator basis with $N_{\text{osc}}^{\text{max}} = 12$ is used. As it is clearly seen, the spectrum is ‘vibrational-like’ (approximately linear energy-vs.-spin dependence) because of the rather small deformation and follow the specific spin-parity combinations in Eq. (3). We have performed calculations with the WS+MI Hamiltonian and obtained very similar results, what justifies the possible use of the schematic interaction for describing the collective excitations.

The previous figure illustrates the results for a rather insignificant deformation of the system of $\alpha_{32} \approx 0.12$. To address the issue of the structure of the rotational bands under the dominating presence of the tetrahedral symmetry, let us consider first a relatively simple case: The nucleus ^{81}Zr , in which one neutron is added on top of the tetrahedral-closed shell $N = 40$ in ^{80}Zr . To guarantee

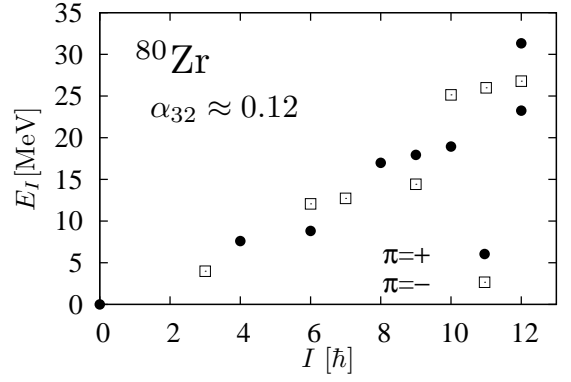


Fig. 2: Preliminary result of calculated excitation spectrum for the tetrahedral ground state of ^{80}Zr calculated with the Gogny D1S interaction.

that tetrahedral symmetry clearly dominates let us consider rather extreme deformation of $\alpha_{32} = 0.4$.

For the half-integer spins the T_d group has three irreducible representations, $E_{1/2}$, $E_{5/2}$ and $G_{3/2}$, where $G_{3/2}$ is four-dimensional, while the others are two-dimensional. In figure 3, we show an example with the valence neutron occupying one of the two-fold degenerate states corresponding to the $E_{1/2}$ representation. It can be seen from the figure that the calculated excitation energies form *two sequences* following the rule $E_I \sim I(I+1)$, thus interpreted as rotational, however, at the same time the tetrahedral symmetry imposes specific ‘extra rules’. These rules are sufficiently characteristic to help defining the strategy of the experimental search of the tetrahedral symmetry in this nucleus and will be discussed in some detail.

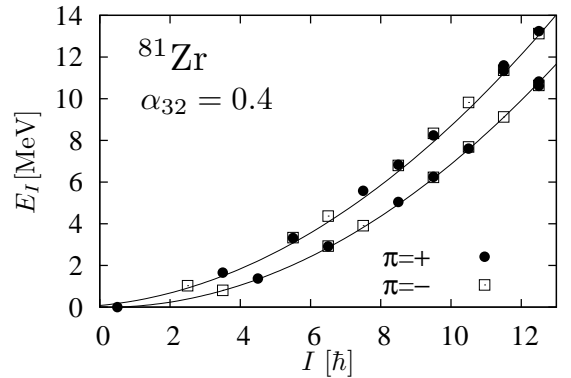


Fig. 3: Calculated spectrum of ^{81}Zr with the WS+MI Hamiltonian; the odd neutron was placed at one of two-fold $E_{1/2}$ levels near the Fermi level. The solid lines connect the energy levels of the rotor including the effect of the Coriolis coupling, cf. eq. (4), and surrounding text.

The projected positive-parity states belonging to the lower branch in figure 3, form a spin-parity sequence beginning with $I^\pi = 1/2^+$, there is no state with $I^\pi = 5/2^+$, the next available state having $I^\pi = 9/2^+$. From now on, the $\Delta I = 2$ sequence is present with the states at $I^\pi = 13/2^+, 17/2^+$, etc. The negative parity sequence begins at the state $I^\pi = 5/2^-$, the ‘expected’ rotational band

member at $9/2^-$ is missing, and instead there are two negative parity states present at $I^\pi = 11/2^-$ and $13/2^-$. The first of them cannot be a band member in the usual sense since there is no $E2$ -transition possible, neither populating nor de-exciting this state within the sequence.

We may conclude that the lower energy branch contains the positive parity band beginning with the band-head at $I^\pi = 9/2^+$ and the negative-parity band beginning with the band-head at $I^\pi = 15/2^-$ only. Such bands could be mistaken with what in a ‘common language’ are called $K = 9/2$ and $K = 15/2$ bands. Observe the symmetry imposed rule of $\Delta I = 3$ ‘spin-shift’ between the two band-heads. Similarly, the upper branch in figure 3 contains $\Delta I = 2$ positive parity sequence beginning with $I^\pi = 7/2^+$ but the negative-parity sequence beginning only at $I^\pi = 13/2^-$, with again $\Delta I = 3$ ‘spin shift’ between the two.

There are yet more characteristic features of the rotational bands in question imposed by the symmetry: Beginning with a certain spin value some members of the band have nearly degenerate opposite parity partners whereas some others have none, within the spin range considered.

Of course the above considerations should be accompanied by the discussion of the characteristic features of the electromagnetic transition probabilities whose branching ratios form another valuable set of criteria for identifying the discussed symmetries in nature, in analogy to the techniques developed in molecular physics. However this part of the discussion is left for a forthcoming publication.

In order to understand the origin of the splitting between the two sequences visible in figure 3, we have considered the conventional particle-rotor model,

$$H_{\text{p-rot}} = E_0 + \frac{I(I+1)}{2\mathcal{J}} - \frac{\mathbf{I} \cdot \mathbf{j}}{\mathcal{J}}. \quad (4)$$

In contrast to the axially-symmetric case, the K quantum number is not the good quantum number in the tetrahedral rotor case, so that it is not totally trivial to evaluate the Coriolis coupling in Eq. (4).

We represent the resultant rotor spectra including the Coriolis coupling by the solid lines in figure 3, where \mathcal{J} is the average moment of inertia parameter of the two projected sequences and E_0 is adjusted in such a way that it shifts the lowest-energy state at zero energy. The matrix elements of \mathbf{j} are calculated with the Woods-Saxon single-particle states. As it is seen from the figure, the splitting between the two parabolic-type sequences can be interpreted as the result of the Coriolis coupling. Note that while the splitting caused by the first order Coriolis coupling is only effective for the $K = 1/2$ -band in the case of the usual axially-symmetric rotor, here the splitting always appears because the coupling parameter is non-zero due to the characteristic K -mixing of the tetrahedral rotor. In the case of the $G_{3/2}$ four-fold degenerate level, the pattern of the coupling is more complicated and the spectra split into more than two sequences; in this case numerical diagonalisation is necessary.

We may conclude that the mean-field calculations with the symmetry projection predict the characteristic splitting of the lowest-lying rotational states into two sequences as the ones in the figure. The presence of these two sequences can be interpreted as the result of the Coriolis effect in odd-A nuclei, when the extra nucleon is added on top of the core with the wave function belonging to the A_1 representation; the details will be reported elsewhere.

For integer-spins the T_d group has five irreducible representations, A_1, A_2, E , and F_1, F_2 , for each of which characteristic spin-parity combinations like the ones in Eq. (3) are assigned, see Appendix of Ref. [6]. The HFB-type states, in which degenerate single-nucleonic levels are occupied with the same probability like in the case of double-closed configuration or of the completely paired configuration in the BCS treatment, belong to the A_1 representation.

In order to analyse, to an extent schematically, the spectra belonging to other irreducible representations, we have performed the following construction: Assuming quenched pairing correlations, we put two neutrons in a four-fold degenerate level, belonging to the $G_{3/2}$ representation, on top of the closed tetrahedral-magic shell in ^{80}Zr at $N = 40$. In order to make the modelling as simple as possible, we use the WS+MI Hamiltonian and choose for this ‘academic’ test as before a rather unrealistically large deformation of $\alpha_{32} = 0.4$, at which the tetrahedral-symmetry effects of the quantum rotor dominate.

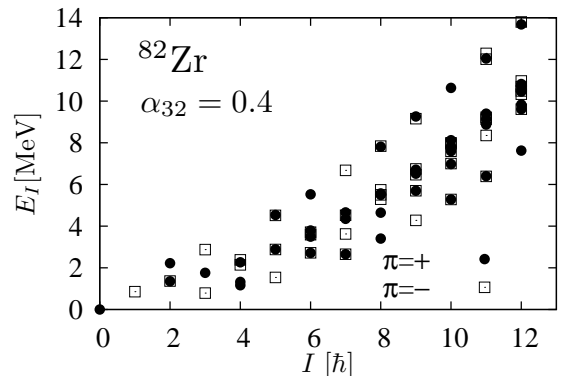


Fig. 4: Low energy levels of ^{82}Zr calculated with the WS+MI Hamiltonian, where two neutrons occupy one of four-fold degenerate $G_{3/2}$ level near the Fermi surface.

We show the resulting spectrum of ^{82}Zr in figure 4. As can be seen, the energy sequences obtained follow clearly the $E_I \sim I(I+1)$ proportionality. The group theory tells us that the coupling of the anti-symmetric two-neutron states of the $G_{3/2}$ -symmetry can be decomposed according to the relation: $\mathcal{A}(G_{3/2} \times G_{3/2}) = A_1 + E + F_2$. It then follows that the resulting energy levels, cf. figure 4 (details are omitted here and are left for the forthcoming publication) belong to one of the three irreducible representations mentioned, i.e., A_1 , E , and F_2 , where the levels belonging to the three-dimensional F_2 -representation split further into three sequences. The detailed analysis and interpretation

of the results in figure 4 can be constructed similarly to the simpler case of ^{81}Zr nucleus discussed above and will not be presented here.

4. High-spin states: Wobbling and Chiral rotations

As the next example, we apply the projection method to the high-spin states focussing on two symmetry-related types of rotational bands, the wobbling- and the chiral-doublet bands. The so-called wobbling bands arise within the quantum mechanical description of the motion of the asymmetric top, see §4-5 of Ref. [4]. In triaxially deformed nuclei the collective rotation about all three principal axes are possible, what results in the phonon-like multiple rotational bands built on top of any single intrinsic configuration. Such multiple band structures have been observed in some of the so-called triaxial superdeformed (TSD) bands in the Lu isotopes, see e.g. Ref. [8].

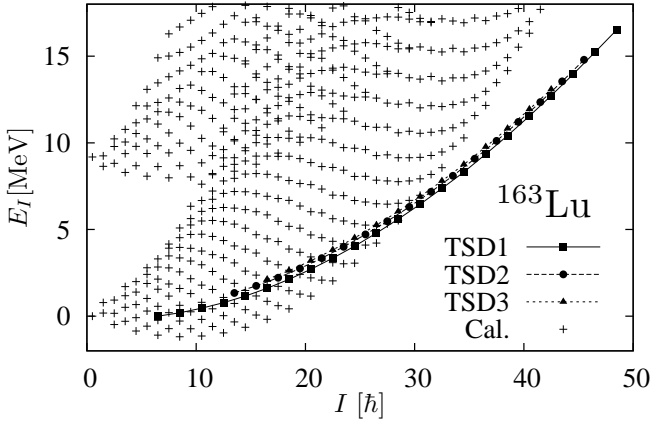


Fig. 5: The results of our projection calculations with the WS+MI Hamiltonian, for the TSD bands in ^{163}Lu . Calculated energy levels marked with the '+'-sign are compared with the experimental results [9] as indicated.

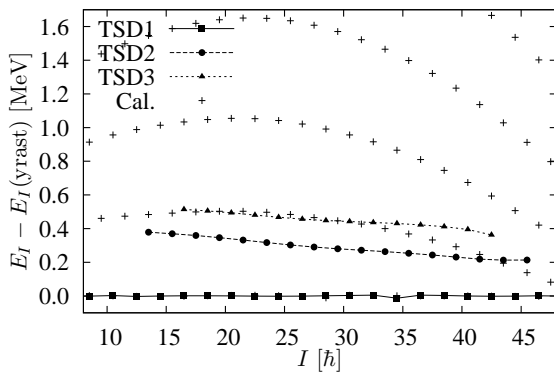


Fig. 6: Relative spectra for the wobbling excitations in ^{163}Lu .

We have performed the angular momentum projection calculations for the TSD bands in ^{163}Lu . In figure 5, we show an example of the spectra calculated with the WS+MI Hamiltonian, and in figure 6 the corresponding

relative excitation spectra. In both figures, the experimentally observed yrast, one-phonon, and two-phonon TSD bands (TSD1, TSD2, and TSD3, respectively) are also included [9]. We also show the results of the out-of-band to in-band $B(E2)$ -ratio in figure 7.

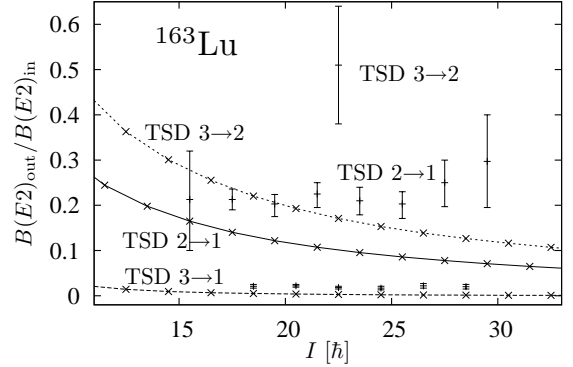


Fig. 7: Calculated $B(E2)$ ratios of the TSD bands in ^{163}Lu are compared with the experimental data [9]

The mean-field deformation parameters used here are $(\beta_2, \beta_4, \gamma) = (0.42, 0.02, 18^\circ)$. They roughly correspond to those of the TSD minima in the Woods-Saxon-Strutinsky calculation. We have chosen the pairing gap parameters $\Delta_n = \Delta_p = 0.5$ MeV. As for the cranking frequency to generate the HFB wave function, we employed $\hbar\omega_{\text{rot}} = 0.2$ MeV, associated with the x -axis cranking. As it is seen from figure 5, a regular multiple band structure appears, however, the calculated moment of inertia of the yrast band is too small compared with the observed one. It should be emphasised that this kind of multiple band structure never appears if the mean-field with too small a triaxiality.

Concerning the results in figure 6, let us note that the relative spectra are rather sensitive to the mean-field parameters, especially to the triaxiality γ and the cranking parameter ω_{rot} . The wobbling phonon excitation energy decreases when increasing γ , while it increases when increasing ω_{rot} . For example, we can reproduce approximately the one-phonon energies either with $\gamma = 30^\circ$ and $\hbar\omega_{\text{rot}} = 0.2$ MeV, or with $\gamma = 18^\circ$ and $\hbar\omega_{\text{rot}} = 0.1$ MeV, although, in the latter case, the excitation energy decreases rapidly and vanishes before spin $40\hbar$. On the other hand, the two-phonon excitation energies can be roughly reproduced with $\gamma = 35^\circ$ and $\hbar\omega_{\text{rot}} = 0.2$ MeV, while we found it difficult to simultaneously reproduce both the one-phonon and two-phonon spectra.

As for the $B(E2)$ ratios in figure 7, the calculated values are smaller than the observed ones; in order to reproduce the ratios larger γ values are necessary. The calculated $B(E2)$ ratio from the one-phonon to the yrast band (TSD $2 \rightarrow 1$) decreases as a function of spin, as long as the constant i.e. spin-independent γ is considered, in contrast to the measured ratio that is almost constant or even increasing. We would like to emphasise that the ultimate features of the wobbling motion, obtained within the

macroscopic rotor model, are satisfactorily reproduced by the present fully-microscopic projection calculation from a single intrinsic wave function, although we are far from its satisfactory description at present.

As another application investigated in this article let us present the chiral rotation studied by employing again the projection method. The chiral doublet bands are predicted for the triaxially deformed nuclei with the proton and neutron angular momenta pointing to two different directions [10]. For example, in the triaxially deformed odd-odd nucleus with an odd proton occupying the high- j particle level and with an odd neutron occupying the high- j hole level, the three angular momentum vectors, that of the proton, of the neutron, and of the collectively rotating nucleus, tend to align with the largest, smallest, and middle principal axes, respectively.

Under these circumstances, after Kelvin, the chirality mechanism arises since the mirror image of an object (nuclear configurations with the three vectors pointing to three directions in space) cannot be superposed with the object itself through rotation. Therefore to each left-handed combination of the three vectors there should correspond a right-handed one with the result that there should always exist two non-identical although chiral-equivalent realisations of each discussed nuclear configuration in a left-handed and right-handed version – of the same energy. However in the quantum systems one can imagine a penetration of the potential barrier separating the two associated potential energy minima with the resulting energy-doublets split or degenerate, depending on the properties of the potential separating the two minima. This mechanism parallels the one of the parity doublet bands in pear-shape octupole-deformed nuclei.

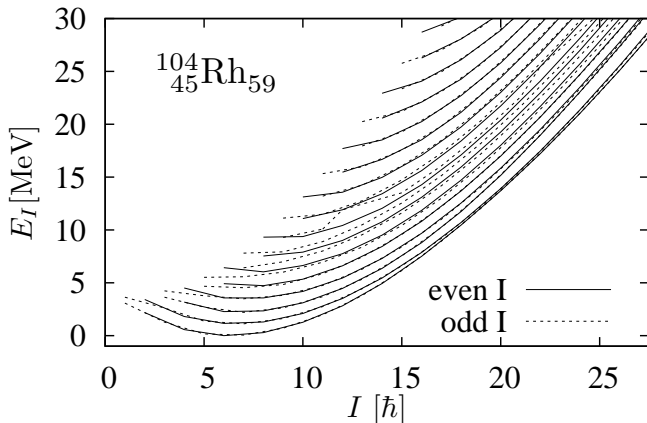


Fig. 8: A result of projection calculation with the WS+MI Hamiltonian for the chiral doublet band in ^{104}Rh .

We wish to verify whether the chiral-doublet bands appear in the calculations with the angular momentum projection applied to the odd-odd nuclei. An example of the results for the ^{104}Rh nucleus is shown in figure 8. In these calculations, we have fixed $\beta_2 = 0.3$ and $\omega_{\text{rot}} = 0$ together with $\beta_4 = 0$ and $\gamma = -30^\circ$ for simplicity. The pairing gaps were self-consistently calculated with the monopole

pairing strengths selected to reproduce the even-odd mass differences for both the neutrons and the protons. Next we have studied the appearance/disappearance of the doublets of bands by changing β_2 deformation and the cranking parameter (ω_{rot} about the x -axis). We found out that the doublet-bands appear within a rather restricted range of β_2 , whereas it seems to be more difficult to obtain degenerate bands when increasing the cranking parameter. As it can be seen from the figure, the odd- and even-spin members are degenerate forming $|\Delta I| = 1$ bands in the lower excitation energy region, and when approaching at high-spins, $I \approx 15 - 30 \hbar$, the two lowest bands produce doublet (rather than fully degenerate) bands, which is expected for the chiral-symmetry breaking.

5. Drip-line nuclei

Finally we have studied rotational properties of certain unstable drip-line nuclei. Our question to examine is: How is the collective rotation affected by the specific features of weak nucleonic binding, the latter manifested through the skin and/or halo mechanisms. To examine this issue, we have chosen the nucleus ^{40}Mg expected to lie close to-, or at the neutron drip-line. According to our Gogny HFB calculations this nucleus has a rather large axial deformation of $\beta_2 \approx 0.34$ in spite of the fact that its neutron number is magic-spherical ($N = 28$). The density distribution indicates that there is a considerable presence of the neutron skin and that the root-mean-square radius, $\sqrt{\langle r^2 \rangle} = 3.63$ fm, i.e. about 15% larger than the that of other stable nuclei in the considered mass range.

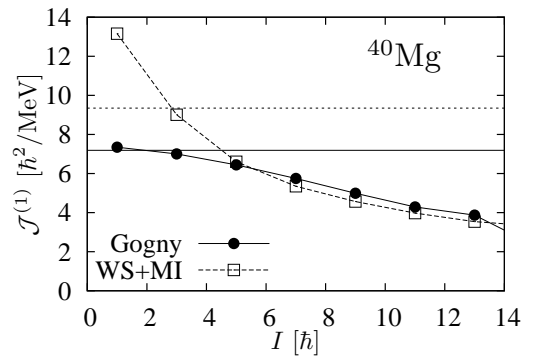


Fig. 9: Preliminary results for the moment of inertia defined as $\mathcal{J}^{(1)} \equiv (2I+1)/(E(I+1) - E(I-1))$ of the ground state band in ^{40}Mg . The horizontal solid (dotted) lines denote the rigid-body values with $r_0 = 1.2$ fm (with the calculated radius).

We have performed the angular momentum projection calculations with both the WS+MI Hamiltonian and the Gogny D1S force. For the WS+MI calculations, we use the deformation parameters calculated by the HFB result with the Gogny D1S force.

Unfortunately, there are not enough experimental data to fix the pairing force strengths in the WS+MI Hamiltonian for ^{40}Mg , so that we used in this paper the data from the stable isotope ^{24}Mg and made the extrapolation to fix

the pairing strengths. This procedure has ambiguities and the resulting spectra depend on the specific choice of the stable isotope being used. The energies of the first 2^+ and 4^+ states are rather sensitive to this choice and may not be very reliable. In figure 9, we show the moments of inertia obtained from the calculated energy levels according to: $\mathcal{J}^{(1)} \equiv (2I+1)/(E(I+1) - E(I-1))$. We have used our two Hamiltonians, both of which give similar results at increasing spins. As it is shown in the figure, the moments of inertia according to both calculations decrease rather rapidly as spin increases. This tendency is very rare for the inertia calculated with the projection method, where the projection is performed from the one HFB-type mean-field state. We think that this feature of the decreasing moment of inertia is specific for the weakly-bound nuclei. Moreover, the value of inertia calculated with the Gogny D1S force is considerably smaller than the rigid-body value even at the lowest spin. This may indicate that the skin and/or halo-like neutron components, whose density distributions tend to be spherical, do not contribute to the moment of inertia of the collective rotation.

6. Summary

We have studied several subjects of contemporary interest in nuclear structure by employing an efficient quantum number projection method, which we have recently developed. The importance of the cranking term is stressed to obtain the correct magnitude of the moment of inertia for the ground state rotational bands.

After applying the projection onto the good angular-momentum as well as parity, we have discussed the rotational band-structures in the tetrahedral-symmetry states of $^{80,81,82}\text{Zr}$. We have formulated some spectroscopic criteria which may be useful when proposing the experiments to test tetrahedral symmetry. Although we have applied the group theory considerations to help understanding the general spectroscopic features, the projection calculations are necessary to obtain the numerical predictions.

Next, the results of the angular momentum projection applied to the high-spin states have been presented. Two kinds of symmetry-related rotational mechanisms, the wobbling bands and the chiral-doublet bands were studied using the fully-microscopic projection calculations.

Finally we have investigated the rotational spectra of the weakly-bound drip-line nuclei, where the effects of the halo and/or skin are expected to be important. The results of our calculation suggest that the moment of inertia of the ground state band in such a drip-line nucleus may decrease with increasing spin, which is quite different from those in the stable nuclei.

Acknowledgement

This work has been partly supported by Grant-in-Aid for Scientific Research (C) No. 22540285 from Japan Society for the

Promotion of Science, and by the Polish-French COPIN collaboration under project number 04-113.

References

- [1] Tagami S and Shimizu Y R, Prog. Theor. Phys. **127**, 79 (2012).
- [2] Ring P and Schuck P, *The nuclear many-body problem* (Springer, New York, 1980).
- [3] Robledo L M, Phys. Rev. **C 79**, 201302(R) (2009).
- [4] Bohr A and Mottelson B R, *Nuclear structure*, Vol. II (W A Benjamin, Inc., 1975).
- [5] J Dudek et al., Phys. Rev. Lett. **88**, 252502 (2002); Phys. Rev. Lett. **97**, 072501 (2006).
- [6] Tagami S, Shimizu Y R and Dudek J, Phys. Rev. **C 87**, 054306 (2013).
- [7] Dudek J and Mazurek K, Nuclear Potential-Energy Data-Base (Strasbourg Cracow Collaboration), http://jacobi.ifj.edu.pl/~mazurek/static/index_alm.php
- [8] Hagemann G, Eur. Phys. J. **A 20**, 183 (2004).
- [9] Jensen D R, Phys. Rev. Lett. **89**, 142503 (2002).
- [10] Frauendorf S and Meng J, Nucl. Phys. **A 617**, 131 (1997).